Physica D 414 (2020) 132708

Contents lists available at ScienceDirect

Physica D

journal homepage: www.elsevier.com/locate/physd

Interaction between vegetation patches and gaps: A self-organized response to water scarcity

M. Tlidi [a,*], E. Berríos-Caro [b], D. Pinto-Ramo [b], A.G. Vladimirov [c], M.G. Clerc [b]

[a] Département de Physique, Faculté des Sciences, Université Libre de Bruxelles (U.L.B.), CP 231, Campus Plaine, B-1050 Bruxelles, Belgium
[b] Departamento de Física and Millennium Institute for Research in Optics, Facultad de Ciencias Físicas y Matemáticas, Universidad de Chile, Casilla 487-3, Santiago, Chile
[c] Weierstrass Institute, Mohrenstrasse 39, 10117 Berlin, Germany

ARTICLE INFO

Article history:
Received 1 September 2019
Received in revised form 20 August 2020
Accepted 27 August 2020
Available online 1 September 2020

Keywords:
Vegetation patterns
localized vegetation patches
self-organization in plant ecology
arid-ecosystems

ABSTRACT

The dynamics of ecological systems are often described by integrodifferential equations that incorporate nonlocal interactions associated with facilitative, competitive interactions between plants, and seed dispersion. In the weak-gradient limit, these models can be reduced to a simple partial-differential equation in the form of a nonvariational Swift–Hohenberg equation. In this contribution, we perform this reduction for any type of kernels provided that their Taylor series converge. Some parameters such as linear and nonlinear diffusion coefficients are affected by the spatial form of the kernel. In particular, Gaussian and exponential kernels are used to evaluate all coefficients of the reduced model. This weak gradient approximation is greatly useful for the investigation of periodic and localized vegetation patches, and gaps. Based on this simple model, we investigate the interaction between two-well separated patches and gaps. In the case of patches, the interaction is always repulsive. As a consequence, bounded states of patches are excluded. However, when two gaps are close to one another, they start to interact through their oscillatory tails. The interaction alternates between attractive and repulsive depending on the distance separating them. This allows for the stabilization of bounded gaps and clusters of them. The analytical formula of the interaction potential is derived for both patches and gaps interactions and checked by numerical investigation of the model equation.

This volume is dedicated to Professor Ehud Meron on the occasion of his sixtieth birthday. We take this opportunity to express our warmest and most sincere wishes to him.

1. Introduction

Spatial fragmentation of landscapes is an inherent characteristic of semi- and arid-ecosystems. In these regions, vegetation populations exhibiting non-random two-phase structures where high biomass density regions are separated by sparsely covered or even bare ground [1]. They cover extensive arid- and semi-arid areas worldwide [2]. The most common is spotted patterns, more or less circular patches surrounded by no plant state, the second consists of bands or arcs (or even spirals), and the third is gaps that are composed of spots of bare soil embedded in a homogeneous cover. The climate of these regions is characterized by water scarcity where the typical annual rainfall lies between 50 and 750 mm. Aridity refers not only to water scarcity but could also be attributed to nutrient-scarce territories. These self-organized structures consist of spatially periodic distributions of patches, stripes, or gaps that occupy the whole space available in a landscape. A transition sequence between this vegetation pattern has been established [3]. As the aridity level is increased, the first pattern that appears consists of a spatial periodic distribution of gaps followed by stripes (or labyrinth) and spots. This generic scenario has been predicted using various ecological models [4–11]. It is widely accepted that facilitative and competitive interactions between individual plants, together with a seed dispersion process provide sufficient conditions for the formation of large scale vegetation patterns [12], that is, biomass has to self-organize to optimize the use of scarce resources.

Vegetation patterns are not always periodic; they can be aperiodic and localized in space. They consist of either localized patches of vegetation, distributed on bare soil [13–18] or, on the contrary, consist of localized spots of bare soil, randomly distributed in an otherwise uniform vegetation cover [19–21]. An example of such a botanical self-organization phenomenon is shown in Fig. 1. This figure illustrates that the phenomenon of self-organization is generic, as it occurs on different spatial scales, kinds of soil, and different types of vegetation. Spatially localized structures or patterns are better known in the contexts of physicochemical rather than biological systems (see overviews [22–32]).

* Corresponding author.
E-mail address: mtlidi@ulb.ac.be (M. Tlidi).

https://doi.org/10.1016/j.physd.2020.132708
0167-2789/

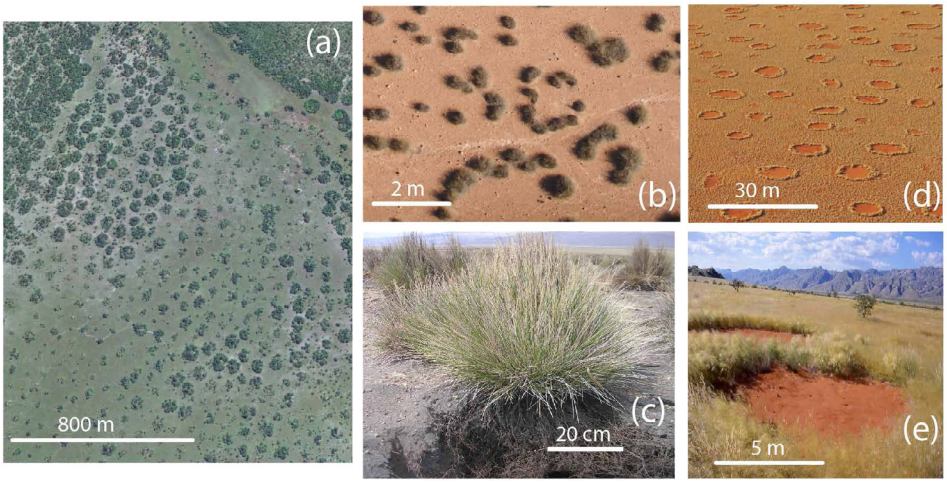

Fig. 1. Localized vegetation patches and gaps. Images of self-organization of localized patches obtained using Google Earth Pro (a, b). (a) Zambia, Southern Africa (13°46′49.07″ S, 25°16′56.97″ E). (b) Ivory Coast, West Africa (7°14′53.01″ N, 6°06′27.83″W). (c) Festuca orthophylla (observed in the Sajama National Park, Bolivia (d, e) Pro-Namibia zone of the west coast of Southern Africa (courtesy of N. Juergen). Random distribution gaps or fairy circles (e) two interacting gaps (photography: courtesy of M. Johnny Vergeer).

We consider the propagation–inhibition type of models under homogeneous and isotropic environmental conditions. The effect of the slope of the ground, water dynamics in surface or in depth, the wind, or the course of the sun is not considered and neglected in this approach. The model allows for the genesis of patterns based solely on the intrinsic dynamics of the vegetation. In other words, the wavelength of the pattern that emerges from the symmetry-breaking instability is intrinsic in the sense that it depends solely on the dynamical parameters such as aridity, and facilitative and competitive interactions ratio. In the first part of this paper, we present a general derivation of a real partial differential equation for the vegetation without any specification of the type of the kernel function associated with facilitative, competitive, and seed dispersion interactions. We show that this model does not depend on the kind of kernel providing that its Taylor series converge. We apply this derivation to Gaussian and exponential type of kernels. In the second part, we investigate the interaction between patches and gaps. Analytical computations allow for the construction of interaction potential between two well-separated localized patches and gaps.

The paper is organized as follows, we present the propagation–inhibition model in Section 2. We derive a real partial differential equation in the form of a nonvariational Swift–Hohenberg model in Section 3. The interaction between two well-separated isolated patches in one and two-dimensional settings is established in Section 4. In Section 5, we review the interaction between gaps and we derive the interaction potential as a function of the modified Bessel function. We conclude in Section 6. A detailed derivation of interaction law between patches in one- and in two-dimensional settings is presented in Appendices A and B.

2. Space–time dynamics of vegetation in scarce environments

The absence of the first principles for biological systems in general, and in particular for ecological ecosystems renders mathematical modeling complex. Most of the mathematical models proposed in the literature are models based on water transport [4,5,33–38]. In contrast, the theory introduced by Lefever and coworkers is grounded on the balance between facilitation and competition interactions exerted by plants themselves, through their above-ground and below-ground parts [12,39–42]. Homogeneous and isotropic environmental conditions are assumed. Besides, no water dynamics either in surface or in depth are assumed. This theoretical approach is a generalization of the paradigmatic logistic Verhulst equation [43–45] with non-local facilitation, competition and seed dispersion [12,19]. This model predicts the fragmentation of a uniform cover when the radius of the root system is larger than the canopy radius, and only when the reproduction processes are cooperative [12]. To satisfy the former condition, the cooperativity parameter often called the feedback balance corresponding to the difference between the strength of the facilitative and competitive interaction should be positive. Indeed, when the aridity level is increased, superficial roots track scarce water or nutrients far beyond the limits of aerial parts of the plant. The wavelength associated with this symmetry breaking instability is intrinsic and depends only on the structural parameters such as the canopy-to-rhizosphere radius ratio. For trees and shrubs, data from arid regions show that the canopy-to-rhizosphere radius ratio may be as small as 1/10. Besides front propagation leading to the stabilization of localized vegetation patches and/or gaps have been reported in [46–52].

The existence of such botanical self-organization is not restricted to a special kind of plant. They may entirely consist of grass, shrubs, or trees (cf. Fig. 1). They are not specific to a special type of soil, which can go from sandy to silty or clayey. To simplify further the modeling of ecosystems, we consider that all plants are mature and we neglect age classes since individual plants grow on a much faster time scale compared to the time scale of the formation of periodic vegetation patterns. The only variable is the vegetation biomass density which is defined at the plant level. The spatiotemporal evolution of the normalized biomass $b(\mathbf{r}, t)$ obeys the following integrodifferential equation

$$\partial_t b = B_1 - B_2 + Dispersion. \tag{1}$$

Time has been scaled such that the characteristic time of the growth process is unity.

The first term $B_1 = b\,(1-b)\,\mathcal{M}_f$, which stands for biomass gain, models the rate at which the biomass increases and saturates. B_1 accounts for biomass productions via dissemination, germination, and other natural mechanisms that tend to increase the biomass. This exponential growth is impossible to maintain over a long time for any population including non cognitive populations such as plants because of the scarcity of resources. The logistic term proportional to $(1-b)$ prevents the biomass production that describes the fact that the biomass cannot exceed the carrying capacity. The nonlocal $M_f(\mathbf{r}, t)$ function describes

interactions facilitating the growth of the biomass such as seed production, germination and other mechanisms that facilitate the increase of biomass density. This positive feedback operates over a distance L_f of the order of the plant's aerial structures (the radius of the crown or the canopy) involving, in particular, a reciprocal sheltering of neighboring plants against arid climatic conditions.

The second term in Eq. (1) represents the biomass losses; $B_2 = -\mu b\mathcal{M}_c$; which describes death or destruction by grazing, fire, termites, or herbivores. The parameter μ measures the resources scarcity often called the aridity parameter. The nonlocal $M_c(\mathbf{r}, t)$ models the plant-to-plant competitive interactions that on the contrary tends to enhance biomass decay. This negative feedback operates over distances of the order of the root length, i.e., the rhizosphere radius L_c. Plants compete through their roots for resources. In other words, the rhizosphere activity of individual plants tends to cut out its neighbors from resources. The plant-to-plant nonlocal interactions are

$$M_{f,c}(\mathbf{r}, t) = \exp\left(\chi_{f,c}\int \phi_{f,c} b(|\mathbf{r}+\mathbf{r}'|, L_{f,c})d\mathbf{r}'\right), \tag{2}$$

where kernels are normalized as $\int \phi_{f,c} d\mathbf{r}' = 1$. The parameters $\chi_{c,f}$ are the interaction strengths associated with the competitive and facilitative, respectively. The parameter μ measures the resource scarcity often called the aridity parameter.

The last term in Eq. (1), describes seed dispersion [19]:

$$\text{Dispersion} = DM_d(\mathbf{r}, t), \tag{3}$$

$$M_d(\mathbf{r}, t) = \int \left[\phi_{in} b(|\mathbf{r}+\mathbf{r}'|, t) - \phi_{out} b(|\mathbf{r}'|, t)\right] d\mathbf{r}', \tag{4}$$

where D is the rate at which plants diffuse, Φ_{in}, and Φ_{out} are the dispersion kernels weighting the incoming and outgoing seed fluxes between neighboring points, according to their distance $|\mathbf{r}'|$.

The kernel function characterizing the nonlocal facilitative–competitive interactions $\phi_{f,c}$, and seed dispersion $\phi_{in,out}$ must satisfy three general conditions: (i) the kernels must be equal to one in the zero biomass limit, i.e., $\lim_{b\to 0}\phi_{f,c,in,out} = 1$, (ii) they should be normalized to ensure that the homogeneous steady states of Eq. (1) are independent of the range of interactions of kernels, i.e., $\int \phi_{f,c,in,out}(|\mathbf{r}'|)d\mathbf{r}' = 1$, and (iii) we assume that the kernels are symmetric and even functions, i.e., $\phi_{f,c,in,out}(|\mathbf{r}'|) = \phi_{f,c,in,out}(-|\mathbf{r}'|)$. At this stage, the spatial shape of the kernel $\phi_{f,c,in,out}(|\mathbf{r}'|)$ has not been yet specified. Generally speaking, kernels can be classified into two types, either weak or strong. If the kernel function decays asymptotically to infinity more slowly (faster) than an exponential function, the nonlocal coupling is said to be strong (weak) [18,53].

By taking into account Eqs. (2), (3), Eq. (1) can be rewritten as

$$\partial_t b = b\,(1-b)\,M_f(\mathbf{r}, t) - \mu b M_c(\mathbf{r}, t) + DM_d(\mathbf{r}, t). \tag{5}$$

We assume that the plants are mature by neglecting the allometric factor that links interaction ranges to biomass density [5,54,55]. The range of facilitative and competitive interactions is thus constant. In addition, we assume homogeneous and isotropic environmental conditions.

The homogeneous steady-state solutions of Eq. (5) are given by

$$\mu = (1-b_s)\exp(\Lambda b_s), \tag{6}$$

where $\Lambda = \chi_f - \chi_c$ is the feedback balance often called the cooperativity parameter.

In the next section, we derive through multiple-scale analysis a simple nonvariational Swift–Hohenberg equation for the vegetation dynamics from the logistic equation with nonlocal interaction between plants Eq. (5). This reduction is valid in the double limit of nascent bistability and close to the vegetation pattern forming threshold. Such a critical point is known as a *Lifshitz point* [56,57], which was initially proposed in the context of magnetic systems [56].

3. A nonvariational Swift–Hohenberg equation for vegetation dynamics

The purpose of this section is to explore the space–time dynamics in the vicinity of the Lifshitz critical point where the homogeneous steady states b_s, solutions of Eq. (6) undergo a second-order critical point marking the onset of a hysteresis loop. At the onset of bistability, the cooperativity parameter is $\Lambda_c = 1$, the biomass density is $b_c = 0$, and the aridity parameter is $\mu_c = 1$. We first define a small parameter ϵ which measures the distance from criticality as

$$\Lambda = \Lambda_c + \Lambda_0\epsilon^{1/2} = 1 + \Lambda_0\epsilon^{1/2}\cdots. \tag{7}$$

We next expand the aridity parameter, as well as the dependent biomass density as

$$\mu = 1 + \mu_0\epsilon + \cdots, \text{ and } b(\mathbf{r}, t) = \epsilon^{1/2}u(\mathbf{r}, t) + \cdots. \tag{8}$$

We expand the strength of the competitive feedback and the scaling for the dispersion coefficient can be written as

$$\chi_c = \chi_0 + \chi_1\epsilon^{1/4} + \cdots, \text{ and } D = p\epsilon^{3/4} + \cdots. \tag{9}$$

Since, we are interested in the regime where the biomass density is small, we can then perform a Taylor expansion of the exponentials appearing in Eq. (2) as

$$M_{f,c}(\mathbf{r}, t) = 1 + \chi_{f,c}\int \phi_{f,c} b(|\mathbf{r}+\mathbf{r}'|, L_{f,c})d\mathbf{r}' + \frac{1}{2}\left(\int \phi_{f,c} b(|\mathbf{r}+\mathbf{r}'|, L_{f,c})d\mathbf{r}'\right)^2 + \cdots. \tag{10}$$

In the same manner, we perform a Taylor expansion of the dispersion kernels $\phi_{in,out}$. The biomass density at the position $\mathbf{r}+\mathbf{r}'$ can expanded as

$$b(\mathbf{r}+\mathbf{r}', t) = b(\mathbf{r}, t) + \left[\mathbf{r}'\cdot\nabla + \frac{1}{2}(\mathbf{r}'\cdot\nabla)^2 + \frac{1}{3!}(\mathbf{r}'\cdot\nabla)^3\right] b(\mathbf{r}, t) + \frac{1}{4!}(\mathbf{r}'\cdot\nabla)^4 b(\mathbf{r}, t) + \cdots. \tag{11}$$

Since the kernel must be normalized and be an even function with respect to the spatial coordinate $\mathbf{r} = (x, y)$, we get

$$\int \phi_{f,c,in} b(|\mathbf{r}+\mathbf{r}'|, L_{f,c,in})d\mathbf{r}' = b(\mathbf{r}, t) + \mathbf{C}_2^{f,c,in}\cdot\nabla^2 b(\mathbf{r}, t) + \mathbf{C}_4^{f,c,in}\cdot\nabla^4 b(\mathbf{r}, t), + \cdots \tag{12}$$

with

$$\mathbf{C}_n^{f,c,in} = \int \phi_{f,c,in}(\mathbf{r}')\frac{\|\mathbf{r}'\|^n}{n!}(\hat{\mathbf{r}}'\cdot\hat{\mathbf{r}})^n\, d\mathbf{r}', \tag{13}$$

where $\hat{\mathbf{r}}'$ and $\hat{\mathbf{r}}$ represent unit vectors. In polar coordinates, $\hat{\mathbf{r}}'\cdot\hat{\mathbf{r}} = \cos\theta$, with θ the angle between them.

We seek corrections to the steady states at criticality that depend on time and space through the slow variables

$$\nabla^2 = \epsilon^{1/4}\tilde{\nabla}^2, \text{ and } \partial_t = \epsilon\partial_{\tilde{t}}/2. \tag{14}$$

Replacing Eqs. (10)–(14) in Eq. (5), and expanding in series of ϵ, the solvability condition at the order $\epsilon^{5/4}$ yields $\chi_0 = C_2^f/(C_2^c - C_2^f)$. At higher order inhomogeneous problem (order $\epsilon^{3/2}$), we obtain the following partial differential equation [19]

$$\partial_t u = -u(\eta - \kappa u + u^2) + (\delta - \gamma u)\nabla^2 u - \alpha u\nabla^4 u, \tag{15}$$

where

$$\eta = 2\mu_0, \kappa = 2\Lambda_0, \delta = 2pC_2^{in}, \gamma = 2\chi_1(C_2^c - C_2^f), \text{ and } \alpha = \frac{2(C_2^f C_4^c - C_2^c C_4^f)}{C_2^c - C_2^f}. \tag{16}$$

Eq. (15) is referred to as a vegetation Swift–Hohenberg equation (VSHE). The coefficients C_2^{in}, $C_2^{f,c}$, and $C_4^{f,c}$ depend on the choice of the kernels used to describe nonlocal facilitative and competitive interactions, $\phi_{f,c}$, and the incoming seed fluxes ϕ_{in}. This dependence is explicitly given by Eq. (13). Therefore, changing the shape of kernel can affect the coefficients C_2^{in}, $C_2^{f,c}$, and $C_4^{f,c}$. Note that the parameters η and κ that describe, respectively, the aridity parameter and the cooperativity, i.e., the feedback balance, do not depend on the coefficients C_i^n. They are independent of the choice of the nonlocal facilitative, competitive, and seed dispersion nonlocal interaction kernels. The parameters δ, γ, and α, describing the vegetation's linear and nonlinear diffusion coefficients depend on the spatial form of the kernel since their values are determined by the coefficients C_i^n. Until now, the shape of the kernels ϕ_i are not yet specified.

Assuming that both the facilitation, competition, and seed dispersion nonlocal interactions are Gaussian [19]:

$$\phi_f = \frac{1}{\pi}\exp(-|\mathbf{r}'|^2), \qquad \phi_c = \frac{\epsilon_1}{\pi}\exp\left(-\epsilon_1|\mathbf{r}'|^2\right), \text{ and } \phi_{in} = \frac{\epsilon_2}{\pi}\exp\left(-\epsilon_2|\mathbf{r}'|^2\right), \tag{17}$$

with $\epsilon_1 = L_a^2/L_c^2$ and $\epsilon_2 = L_a^2/L_d^2$. For the Gaussian kernel we have

$$\delta = \frac{p}{2\epsilon_2}, \gamma = \frac{\chi_1(1-\epsilon_1)}{2\epsilon_1}, \text{ and } \alpha = \frac{1}{16\epsilon_1}$$

When both the facilitation, competition, and seed dispersion nonlocal kernels are exponentials:

$$\phi_f = \frac{1}{2\pi}\exp(-|\mathbf{r}'|), \qquad \phi_c = \frac{\epsilon_1^2}{2\pi}\exp\left(-\epsilon_1|\mathbf{r}'|\right), \text{ and } \phi_{in} = \frac{\epsilon_2^2}{2\pi}\exp\left(-\epsilon_2|\mathbf{r}'|\right), \tag{18}$$

with the normalization coefficient

$$\int \phi_{c,f,in}(\mathbf{r}')\mathrm{d}\mathbf{r}' = 1, \tag{19}$$

performing integrals from Eq. (13) using polar coordinates, and after straightforward calculations we obtain: $C_2^f = 3/2$, $C_2^c = 3/(2\epsilon_1^2)$, $C_2^{in} = 3/\epsilon_2^2$, $C_4^f = 15/8$, and $C_4^c = 15/(8\epsilon_1^4)$, and by replacing these coefficients in Eq. (16), we get

$$\delta = \frac{3p}{2\epsilon_2^2}, \quad \gamma = \frac{3\chi_1}{\epsilon_1^2}(1-\epsilon_1^2), \quad \text{and} \quad \alpha = \frac{15}{8\epsilon_1^2}. \tag{20}$$

Note that in the case of a strong nonlocal coupling such as a Lorentzian, the Taylor series does not converge, and the integrals describing the nonlocal interactions cannot be expressed as a gradient expansion. Therefore, in this case, the above real order parameter description leading to the derivation of the simplified model VSHE Eq. (15) cannot be applied. The real order parameter VSHE has been first derived in [3]. A detailed derivation of VSHE using a multiple-scale analysis has been reported in [19] where nonlocal interactions have been considered as Gaussian. Recently, the VSHE has been recovered [58] by using the water-limited vegetation model proposed by Meron and collaborators [59]. Other variational type of Swift–Hohenberg equation has been derived in the context of fluid mechanics [60] and since then it constitutes a paradigmatic model in the study of the periodic and localized patterns. It has been derived for that purpose in other fields of natural science, such as electroconvection [61], mechanics [62,63], chemistry [64], plant ecology [41,42,65–67], and nonlinear optics [68–70].

The homogeneous steady states solutions of VSHE satisfy $u_0 = 0$, and $u_\pm = (\kappa \pm \sqrt{\kappa^2 - 4\eta})/2$. The spatially uniform bare state b_0 corresponds to a state devoid of vegetation. The homogeneously covered vegetation state is denoted by u_+. These two states are separated by an unstable homogeneous cover with lower biomass density u_-. The homogeneous vegetated states exhibit a symmetry-breaking instability at $u = u_c$ with an intrinsic wavelength explicitly given by the following simple relation

$$\lambda = 2\pi\sqrt{\frac{2\alpha u_c}{\gamma u_c - \delta}}, \tag{21}$$

where u_c satisfies

$$4\alpha u_c^2(2u_c - \kappa) = (\gamma u_c - \delta)^2. \tag{22}$$

This relation determines the threshold state at which the symmetry-breaking instability appears on the u_+ branch of solutions. This instability can be seen from the vegetation effective diffusion coefficient, i.e., $(\delta - \gamma u)$, which multiplies the Laplace operator ∇^2 in the VSHE may become negative. This sign change in the effective diffusion, tends to destabilize the spatial uniformity of the vegetation biomass density. The bi-Laplacian ∇^4 term is always stabilizing since its coefficient, $-\alpha u$ is always negative.

4. Interaction between localized patches

In a regime where the homogeneous cover coexists with periodic vegetation patterns, localized patches can be stabilized in a finite range of the aridity parameter often called the pinning zone. A single localized patch is more or less of a circular shape in homogeneous and isotropic environmental conditions. We focus on the regime where a single patch is stable, and we shall investigate in a detailed way the interaction between two well separated patches. The interaction between localized vegetation gaps and patches in arid and semi-arid landscapes has received a limited attention [19,71–73]. It has been shown that the interaction between localized vegetation patches is always repulsive [73], and therefore localized patches bound states of vegetation are not possible [73]. The repulsive nature of the interaction together with boundary conditions allows for the coexistence of several vegetation patterns with different wavelengths [73]. This repulsive nature has been reported previously in a prototype model for population dynamics with a nonlocal interaction [74].

4.1. Interaction between localized patches in 1D

We first address the problem of the interaction between patches in a one-dimensional setting. A single localized patch $u(x)$ is a solution of the VSHE. The asymptotic behavior of the tail can be estimated since a localized patch has a small amplitude far from its center, i.e., when x is large. We perform a linear analysis around the homogeneous bare state $u = 0$ by linearizing in u, we get $0 = -u\eta + \delta\partial_{xx}u$. The solution of this linear equation is

$$u\,(|x - x_0| \to \infty) \qquad \propto e^{-\beta|x-x_0|}, \qquad \text{with } \beta = \sqrt{\eta/\delta}, \tag{23}$$

where x_0 is the center position of localized patch as depicted in Fig. 2. The previous asymptotic behavior is confirmed numerically by performing a curve fitting in the tails. A single localized patch is a stationary solution of the VSHE, which can be interpreted as a nonlinear front that undergoes a pinning effect between the spatially periodic vegetation pattern and the bare state [13]. The size of an isolated patch is intrinsically determined by the vegetation dynamics and not by the spatial variation of the environment. It neither grows in spite of available free space, nor decreases in

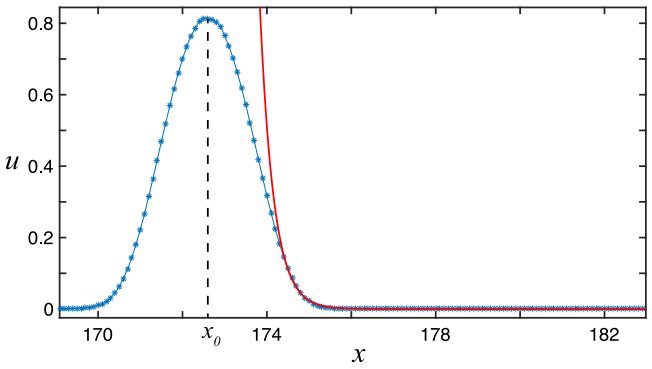

Fig. 2. One dimensional localized structure profile obtained numerically from Eq. (15). The parameters used are $\eta = 0.17$, $\kappa = 0.8$, $\delta = 0.02$, $\gamma = 0.5$, and $\alpha = 0.13$. The red line corresponds to the exponential fitting $R0(t)/w = (1/)ln(At)$, using Eq. (23). Theoretical value of γ is 2.91 and from the fitting 3.06. The coefficient of determination results in $R^2 = 0.9978$.

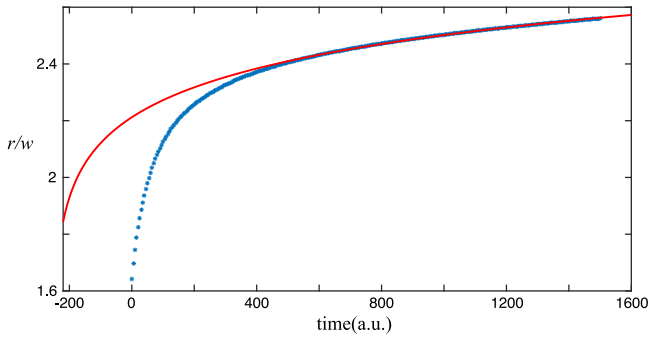

Fig. 4. Curve fitting of numerical data of $r(t)$. The red curve is the fitting obtained using Eq. (26). The parameters used were $\eta = 0.12, \kappa = 0.6, \delta = 0.02, \gamma = 0.5$, $\alpha = 0.125$, $dt = 0.01$, and $dx = 0.4$. (For interpretation of the references to color in this figure legend, the reader is referred to the web version of this article.)

spite of adverse conditions [13]. However, when two localized patches are initially at a certain distance from each other, they start to move, repelling each other. This repulsion is presented in Fig. 3(b), where we have measured numerically the distance of separation $r(t)$ as a function of time. We have considered r as the distance between the center positions of both interacting patches. The time evolution of r obeys a logarithmic rule, implying that its temporal derivative follows an exponential law in r ($\dot{r} \propto e^{-Ar}$), which makes sense since the asymptotic behavior of the single patch tails is exponential. In the next section, we will derive analytically the dynamic equation that r satisfies in a particular limit and will compare with numerical data. In what follows we derive the interaction potential between two localized patches. For this purpose, we consider a linear superposition of two stationary localized patches u_1 and u_2 located at the positions x_1 and x_2 separated by a distance $r(t) = x_2 - x_1$,

$$u(x,t) = u_1(x - x_1(t)) + u_2(x - x_2(t)) + W(x_1(t), x_2(t), x), \qquad (24)$$

where the function W accounts for the corrections due to the interaction forces, which will be assumed small. The terms proportional to the product of W with $\dot{x}_-(t)$ or $\dot{x}_+(t)$ will be neglected, since patches move on a slow time scale. In addition, we assume that the distance r is large compared to the size of a single localized patch. Therefore, introducing this ansatz into the corresponding one dimensional VSHE, after straightforward calculations (see Appendix A), and by using the solvability condition, we get Eq. (A.23). For large r, the term $\exp(-2\beta r)$ can be neglected, and Eq. (A.23) reads

$$\partial_t r = A \exp(-\beta r), \qquad (25)$$

where A is given by Eq. (A.24). The solution of Eq. (25) is

$$r(t) = \frac{\ln(A\beta)}{\beta} + \frac{\ln(t - t_0)}{\beta}. \qquad (26)$$

The distance between two separated localized patches evolves in time according to a logarithmic law. This simple formula is checked with the direct numerical simulations of the governing equation as shown in Fig. 4. The obtained value of tail decay rate associated with localized vegetation patches is $\beta = 2.40$, which is in a very good agreement with the theoretical value $\beta = (\eta/\delta)^{1/2} = 2.45$.

In the course of time, the distance between two localized patches increases. Therefore, bound states of patches are not allowed. As a consequence, the wavelength of a periodic train of peaks depends strongly on the system size. When a small random initial condition is used, in the course of time, the system reaches a periodic structure (see left panel of Fig. 5). If however, we remove one or two peaks, the system will reach a stable periodic pattern with a bigger wavelength as shown in Fig. 5(b) and (c), respectively. These figures have been obtained for fixed values of the parameters, they differ only by the initial conditions. In the next subsection we discuss the interaction in the two-dimensional system.

4.2. Interaction between localized patches in 2D

In the previous subsection we have shown that in one dimensional systems, the interaction between well-separated localized patches follows an exponential law. In what follows, we focus on the two-dimensional interaction problem. The single stationary isolated patch is a solution of the linearized problem around

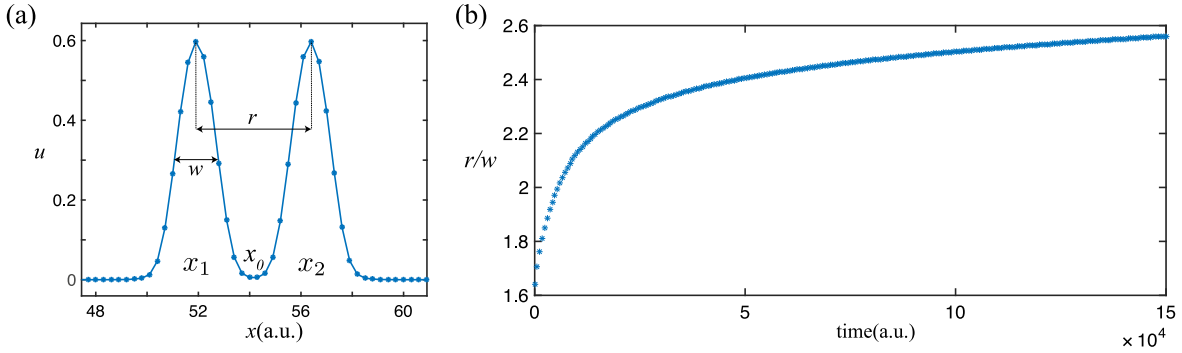

Fig. 3. (a) Two localized patches separated by a distance r. (b) Numerical data of r as a function of time, showing the repulsion between patches. The parameters are $\eta = 0.12$, $\kappa = 0.6$, $\delta = 0.02$, $\gamma = 0.5$, $\alpha = 0.125$, and $dx = 0.4$.

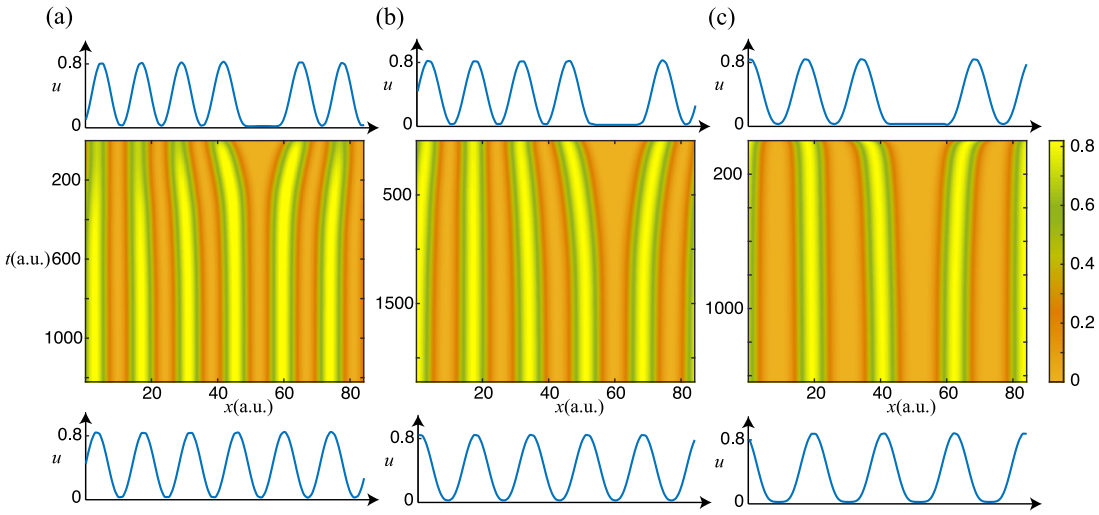

Fig. 5. Evolution of periodic one-dimensional configurations, after removing one localized structure. The figures (a), (b) and (c) show the evolution of a seven, six, and five periodic profile evolution, after removing one patch. The upper and lower profiles show the initial and final profile of each case, respectively. In all cases the patches rearrange, reaching a new periodic profile with a larger wavelength. The parameters used were $\eta = 0.13$, $\kappa = 0.7$, $\delta = 0.01$, $\gamma = 0.5$, $\alpha = 0.1$, $dx = 0.26$ and $dt = 0.01$.

the bare state. Since localized solution has a radial symmetry, it is then convenient to express the Laplace operator in spherical coordinates i.e., $\nabla^2 = (1/r)\partial_r + \partial_r^2$. The resulting linear problem admits an analytical solution

$$u(r) = AK_0(\beta r), \tag{27}$$

where $A > 0$ is a constant, $\beta = \sqrt{\eta/\delta}$, and K_0 is the modified Bessel function of second kind, which is a real function for $r > 0$. For large values of r we can approximate this function by

$$K_0(r) \approx \sqrt{\frac{\pi}{2}}\frac{e^{-r}}{\sqrt{r}}, \tag{28}$$

and then,

$$u_{LS}(r \to \infty) \propto \frac{e^{-\beta r}}{\sqrt{r}}, \tag{29}$$

which describes the asymptotic behavior of the two dimensional localized patches tails. If two or more patches are close to one another they interact through their tails. An example of two interacting localized patches is illustrated in Fig. 6.

To simplify further the analysis, we suppose that the maxima of the patches are located, respectively, at the points $(-r/2, 0)$ and $(r/2, 0)$ and along the x direction, where r is the distance between the two localized patches. To study this interaction, we add a small perturbation $W = W(r, \mathbf{x})$ to the linear superposition of the two interacting patches separated by a distance r

$$u(\mathbf{x}, t) = u_1(\mathbf{x} + r(t)/2) + u_2(\mathbf{x} - r(t)/2) + W(r, \mathbf{x}), \tag{30}$$

where $\mathbf{x}$ accounts for the two-dimensional vector, u_1 and u_2 stand for two localized structures separated by a distance r. Performing an analysis similar to that in the previous section, we obtain

$$\dot{r} = A\frac{e^{-\beta r}}{\sqrt{r}} \tag{31}$$

where A is defined in (A.24).

Fig. 7 presents a curve fitting of $\dot{r}$ as a function of r obtained numerically. The fitting is performed by considering Eq. (31), assuming that r is large. As is the 1D case, the distance between two interacting patches is always increasing during time evolution. Therefore, stable 2D bounded patches are unstable since the interaction is always repulsive.

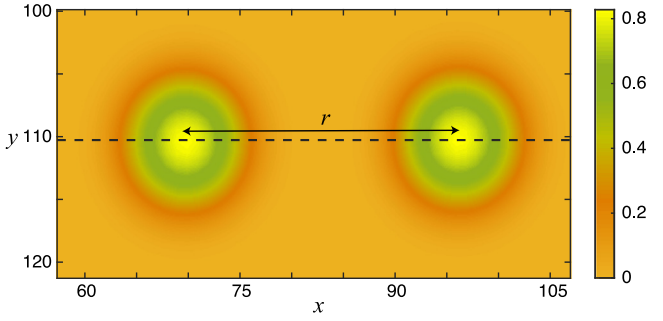

Fig. 6. Two-dimensional structures located at a distance r. The dashed line passes through the centers and will be the axis where we restrict our calculations. The parameters are $\eta = 0.12$, $\kappa = 0.6$, $\delta = 0.02$, $\gamma = 0.5$, $\alpha = 0.125$, $dx = dy = 0.3$, and $dt = 0.001$.

5. Interaction between gaps

In contrast with localized patches where the interaction is always repulsive, we shall see that gaps interact in a different way. It has been shown that depending on the distance separating the two gaps, the interaction alternates between attractive and repulsive [19]. We will first perform numerical simulations showing stable bound states of gaps. Second, we will review the interaction law governing the interaction between two well separated gaps [19]. In particular, we will review and derive an explicit analytical expression for the interaction potential between two-gaps as a function of the modified Bessel function. As we shall see, this function describes the damped oscillatory tail of the interacting gaps.

To generate a stable circular gap, we have to apply initially a perturbation with zero biomass density on the uniformly vegetated cover. If one applies initially this perturbation at two different locations in space, two localized gaps are formed separated by some distance. The two gaps start to interact, and in the course of time, they either repel or attract each other depending on the initial distance separating them. As in the case of patches, the interaction between gaps evolves on a very long-time scale. Numerical simulations of the VSHE shows three examples of the stable equilibrium state corresponding to a stationary bound state of gaps (see Fig. 8). Numerical results indicate that there

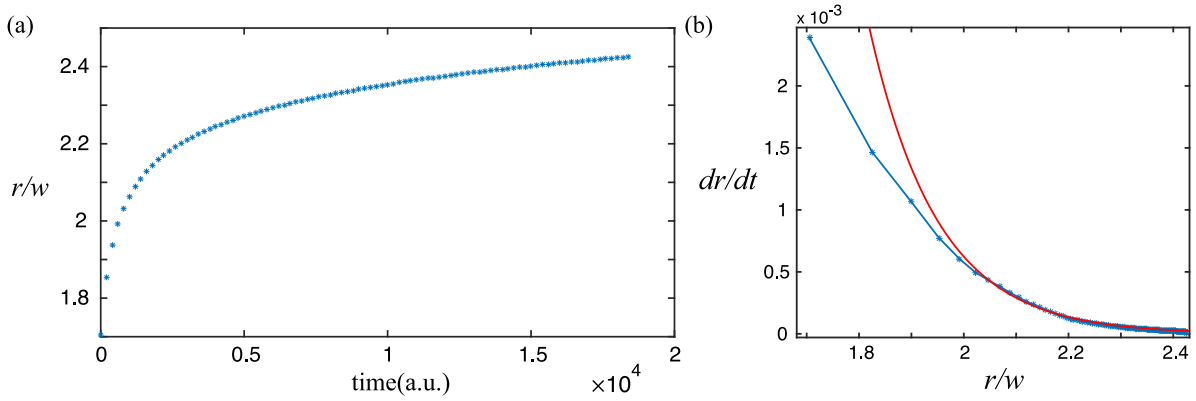

Fig. 7. (a) Numerical data of the distance of separation r in function of time, in units of the width w. (b) Curve fitting of numerical data of $\dot{r}$ as a function of r, using first term of Eq. (31). The distance r is normalized with the localized patches width. The parameters are the same as in Fig. 7.

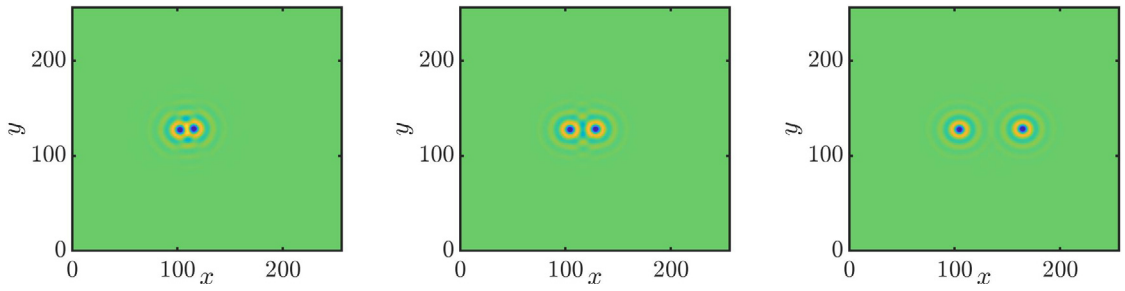

Fig. 8. Examples of stable two-bounded localized patches obtained by numerical simulations of Eq. (15) with periodic boundary conditions in both x and y spatial coordinates. These bounded solutions are obtained for the same values of parameters. They differ only in the initial distance between the two interacting patches. The parameters are $\kappa = 0.5$, $\delta = 0.01$, $\gamma = 0.5$, $\alpha = 0.1$, and $\eta = -0.05$.

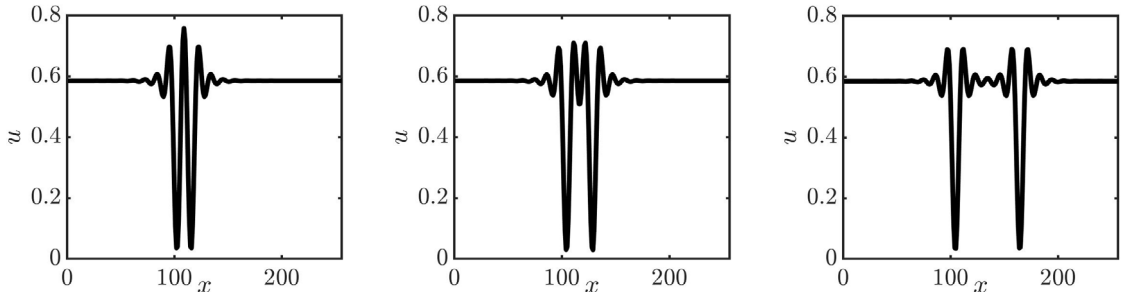

Fig. 9. Spatial profiles of the 2D gaps along the x. Three cross sections have been taken from (Fig. 8).

exist several stable equilibrium positions. The three equilibrium positions are obtained for the same values of the parameters and for the same boundary conditions, and they differ only in the initial distance between the two gaps. The spatial profile along the x direction shows clearly that gaps possess damped oscillatory tails [see cross sections depicted in Fig. 9].

A single localized gap is a radially symmetric solution $u(x, y) = u(r)$ of the VSHE. This localized state possesses an oscillatory tail, which can be calculated using the fact that the gap amplitude is close to the homogeneous cover u_+ far away from its center, i.e., when r is large. Therefore, in order to calculate the asymptotic behavior of the gap solution we substitute into Eq. (15) an expression $u(\mathbf{r}, t) = u_+ + U(r)$ and by linearizing this equation around u_+, we obtain

$$\nabla^2 \begin{pmatrix} U \\ V \end{pmatrix} = M \begin{pmatrix} U \\ V \end{pmatrix} \quad M = \begin{pmatrix} 0 & 1 \\ -\xi_2 & \xi_1 \end{pmatrix}, \tag{32}$$

where $V = \nabla^2 U$, $\xi_1 = (\delta - \gamma u_+)/(\alpha u_+)$, and $\xi_2 = (3u_+^2 + \eta - 2\kappa u_+)/(\alpha u_+)$. The solution of this equation gives the asymptotic behavior of the localized gap in terms of the modified Bessel function K_0:

$$\begin{pmatrix} U \\ V \end{pmatrix} \approx A\{\vec{v}\exp(i\theta)K_0\left[(\omega_1 + i\omega_2)r\right] + c.c.\}, \tag{33}$$

where $\omega_1 \pm i\omega_2 = \left[\xi_1/2 \pm i\sqrt{\xi_2 - (\xi_1/2)^2}\right]^{1/2}$ are complex eigenvalues, while $\vec{v} = \left[1 \quad (\omega_1 + i\omega_2)^2\right]^T$ and $\vec{v}^* = \left[1 \quad (\omega_1 - i\omega_2)^2\right]^T$ are complex eigenvectors of the matrix M. Real constants A and θ must be calculated numerically.

Two or more localized vegetation gaps will interact through their overlapping tails if they are close enough. The interaction between localized states is a well documented issue in contexts of a physico-chemical systems [75–79] rather than biological systems [19]. We consider the simplest situation where the two identical and radially symmetric interacting gaps are located at the positions $\mathbf{r}_{1,2}$. Without the loss of generality, we assume that the positions of both gaps are on the x-axis, i.e., their minima are located at the points $(-R/2, 0)$ and $(R/2, 0)$, where $R = |\mathbf{r}_2 - \mathbf{r}_1|$

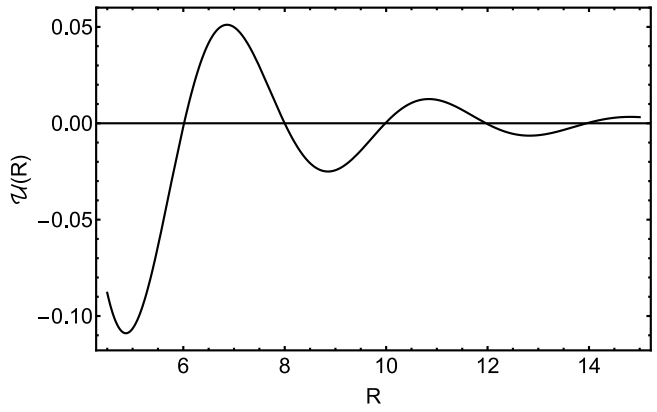

Fig. 10. Interaction potential as a function of the distance R between two localized gaps. Parameters are $\kappa = 0.5$, $\delta = 0.01$, $\gamma = 0.5$, $\alpha = 0.1$, and $\eta = -0.05$.

is the distance between the gaps. In the regime of week overlap, we look for the solution of the VSHE in the form of slightly perturbed linear superposition of two gaps:

$$u(\mathbf{r},t) = u_+ + U_1(\mathbf{r}) + U_2(\mathbf{r}) + \varepsilon\delta u(\mathbf{r},t) \quad \text{where}$$
$$U_{1,2}(\mathbf{r}) = U\left(|\mathbf{r} - \mathbf{r}_{1,2}|\right), \tag{34}$$

where their positions $\mathbf{r}_{1,2}$ evolve on the slow time scale εt. The time evolution of the distance between two-identical gaps can be calculated by substituting Eq. (34) into Eq. (15), collecting first order terms in ε, and writing the solvability condition of the resulting linear equation [19]

$$\partial_t \mathbf{R} = -\nabla_{\mathbf{R}} \mathcal{U}(R), \tag{35}$$

where the potential function

$$\mathcal{U}(R) = 4\alpha u_+ \left[\xi_1 \int_{\infty}^{\infty} (U_x U)_{x=R/2}\, dy - \int_{-\infty}^{\infty} (UV_x + U_x V)_{x=R/2}\, dy\right]. \tag{36}$$

Here $U_x(r)$ is the x-component of the eigenfunction of the linear operator $\mathcal{L}^\dagger$ adjoint to the operator $\mathcal{L}$, which is obtained by linearizing Eq. (15) around the gap solution $U(r)$ and $V(r) = \nabla^2 U(r)$. The asymptotic behavior of U_x and $V_x = \nabla^2 U_x$ at large r is given by

$$\begin{pmatrix} U_x \\ V_x \end{pmatrix} \approx B\left(\frac{x}{r}\vec{v}\exp(i\varphi)K_1\left[(\omega_1 + i\omega_2)r\right] + c.c.\right), \tag{37}$$

where real constants B and φ must be calculated numerically. A detailed derivation of Eq. (36) as well as the evaluation of the integrals $I_{1,2}$ can be found in the book chapter [19]. After substituting asymptotic relations (33) and (37) into Eq. (36), and performing integration we finally get:

$$\mathcal{U}(R) = -8\pi AB\alpha u_+ \Im\left(\frac{\omega_1\omega_2 e^{i(\theta+\varphi)}}{(\omega_1 + i\omega_2)^2} K_0\left[(\omega_1 + i\omega_2)R\right]\right). \tag{38}$$

The minima (maxima) of the interaction potential corresponds to stable (unstable) localized gaps bound states, where two bare spots are bounded together by the interaction force. The interaction potential (38) associated with two-gaps is plotted in Fig. 10. From this figure, we see that there is a discrete set of stable and unstable bounded vegetation patches. Numerical simulations were conducted using the finite differences scheme with Runge–Kutta order-4 algorithm and periodic boundary conditions.

6. Conclusions

A nonlinear model for population dynamics is introduced to describe the interaction and propagation of vegetation in arid and semi-arid environments. The nonlocal facilitative and competitive interactions between individual plants together with seed dispersion have been explicitly incorporated into the model. Starting from this integro-differential model, we have derived a simple partial differential equation in the form of a non-variational Swift–Hohenberg equation. This derivation is valid in the double limit: close to the critical point associated with bistability, and close to the long wavelength pattern forming regime.

In the first part, we have performed this derivation without any specification of the form of kernels used to describe nonlocal interactions between plants. The originality of the results presented in this contribution resides in the fact that the derivation of the vegetation Swift–Hohenberg model is kernel independent. This derivation is rather general but its application is limited to kernels whose Taylor series converge. We have shown that parameters δ, γ, and α, describing vegetation diffusion coefficients depend on the spatial form of the kernel, while the aridity parameter and the feedback balance, do not depend on the type of the kernels used. The Gaussian and exponential type kernels have been used to estimate the model parameters.

In the second part, we have discussed the formation of localized patches and gaps including their interaction. In particular, we have presented a detailed derivation of the law governing the interaction between two well-separated patches. A single patch surrounded by the no plant state and connecting this state to the spatially periodic pattern, is stable over a large range of the aridity parameter [13]. The tail of the patch is monotonously decaying as a function of the distance from its center, i.e., devoid of damped spatial oscillations. This is because the biomass density is a positively defined quantity and therefore damped oscillations around the no plant state are physically not possible. It has been shown recently that when two patches are sitting on bare terrain (with zero total biomass), they interact in a repulsive way, and obviously, the repulsive nature of such interaction prevents the formation of bounded localized patches. In this work, the interaction between patches has been analyzed especially in connection with the coexistence of stable vegetation patterns with different wavelengths. The repulsive nature of such interaction affects not only the vegetation pattern formation process but also the pattern selection since it allows for the stabilization of new extended vegetation patterns such as squares and superlattices [73]. In the present paper, we performed a more extensive analysis of the interaction between vegetation patches in one and two-dimensional settings. A detailed analysis has been presented in Appendices A and B.

In the last part, we have investigated the interaction between gaps. Gaps have been generated in a regime where a uniformly vegetated cover coexists with a periodic vegetation pattern. In contrast with patches, localized gaps possess a damped oscillatory tail, which affects the laws governing their interaction. It has been shown that the interaction alternates between attractive and repulsive depending on the distance separating the gaps [19]. The existence of a discrete stable equilibrium position allows for the stabilization of bound states and clusters of gaps. We have constructed the interaction potential, and we have improved the results of Ref. [19] by deriving an explicit analytical expression for the interaction potential of two weakly overlapping gaps in terms of the modified Bessel function.

Declaration of competing interest

The authors declare that they have no known competing financial interests or personal relationships that could have appeared to influence the work reported in this paper.

Acknowledgments

We would like to thank R. Lefever for helpful interactions. We are grateful to S.S. Gopalakrishnan for his continuous help. M.G.C. thanks for the financial support of FONDECYT projects 1180903 and Millennium Institute for Research in Optics (MIRO). M.T. acknowledges support as a Research Director with the Fonds de la Recherche Scientifique F.R.S.-FNRS, Belgium. The authors gratefully acknowledge the financial support of Wallonie-Bruxelles International (WBI).

Appendix A. Derivation of the interaction potential in 1D

We derive the interaction law of two localized structures separated by a distance $r(t) = x_2(t) - x_1(t)$, with the central position or centroid $x_0 = (x_2(t) - x_1(t))/2$ [see Fig. 3(a)]. Let us first introduce the ansatz presented in Eq. (24) into Eq. (15), i.e. the dynamical equation of the system, and derive a linear system in W, the correction term. Recall that $x_1(t)$ and $x_2(t)$ account for positions of structures u_1 and u_2, respectively. Notice that they have been promoted as functions of time. Our aim in this section is to derive dynamical equations for $r(t)$ and $x_0(t)$ under certain assumptions.

As mentioned in the main text, it is assumed that the term W is small, i.e. nonlinear terms are neglected. Moreover, the localized structure is assumed to travel slow enough so that the terms proportional to the product of W with either $\dot{x}_1$ or $\dot{x}_2$ are not considered. Therefore, under the previous assumptions, the linear system associated to W becomes

$$\mathcal{L}W = b, \tag{A.1}$$

with the linear operator $\mathcal{L}$ defined as

$$\begin{aligned}\mathcal{L} = &-\eta + 2\kappa(u_1+u_2) - 3(u_1+u_2)^2 + \delta\partial_{xx} \\ &- \gamma\left[(u_1+u_2)\partial_{xx} + \partial_{xx}(u_1+u_2)\right] \\ &- \alpha\left[(u_1+u_2)\partial_{xxxx} + \partial_{xxxx}(u_1+u_2)\right],\end{aligned} \tag{A.2}$$

and

$$\begin{aligned}b = &\frac{\dot{r}}{2}\left(\partial_{z_1}u_1 - \partial_{z_2}u_2\right) - \dot{x}_0\left(\partial_{z_1}u_1 + \partial_{z_2}u_2\right) \\ &- 2\kappa u_1u_2 + 3u_1u_2\,(u_1+u_2) \\ &+ \gamma\,(u_1\partial_{xx}u_2 + u_2\partial_{xx}u_1) \\ &+ \alpha\,(u_1\partial_{xxxx}u_2 + u_2\partial_{xxxx}u_1)\,.\end{aligned} \tag{A.3}$$

where u_1 and u_2 are stationary gaps solutions of Eq. (15). The time evolution of the distance separating the two interacting gaps $\dot{r}$ as well as the time evolution of the central position $\dot{x}_0(t)$ will be derived by applying the Fredholm solvability condition, for the following inner product

$$\langle f|g\rangle = \int_{-\infty}^{+\infty} f(x)g(x)\,\mathrm{d}x, \tag{A.4}$$

with $f(x)$ and $g(x)$ as real-valued functions. The derivation of the associated adjoint operator $\mathcal{L}^\dagger$ is necessary for applying this condition.

A.1. Adjoint of $\mathcal{L}$

To obtain $\mathcal{L}^\dagger$, we take a look at the property $\langle\mathcal{L}^\dagger f|g\rangle = \langle f|\mathcal{L}g\rangle$ for adjoint operators. From here, it is straightforward to see that the terms of $\mathcal{L}$ remain the same as in $\mathcal{L}^\dagger$, except

$$\gamma(u_1+u_2)\partial_{xx} \quad \text{and} \quad \alpha(u_1+u_2)\partial_{xxxx}. \tag{A.5}$$

The adjoint of these terms can be obtained by integrating by parts. We illustrate this procedure for the first of them.

When introducing $\gamma(u_1+u_2)\partial_{xx}$ into the inner product

$$\langle f|\gamma(u_1+u_2)\partial_{xx}g\rangle = \int_{-\infty}^{+\infty} f(x)\,\gamma\,[u_1(x)+u_2(x)]\,\partial_{xx}g(x)\,\mathrm{d}x, \tag{A.6}$$

and integrating by parts once, we get

$$f(x)\gamma\,[u_1(x)+u_2(x)]\,\partial_{xx}g(x)\Big|_{-\infty}^{\infty} - \int_{-\infty}^{+\infty}\partial_x[f(x)\gamma(u_1(x)+u_2(x))]\partial_x g(x)\mathrm{d}x. \tag{A.7}$$

The time dependence of u_1 and u_2 has been suppressed for simplicity of notation. The first of these terms vanishes, as (u_1+u_2) tends to zero as $x \to \pm\infty$. Integrating by parts once more, and proceeding in a similar way, we get

$$\langle f|\gamma(u_1+u_2)\partial_{xx}g\rangle = \langle\partial_{xx}[f\ \gamma(u_1+u_2)]|g\rangle, \tag{A.8}$$

so that, the corresponding element of $\gamma(u_1+u_2)\partial_{xx}$ in $\mathcal{L}^\dagger$ takes the form $\partial_{xx}[\gamma(u_1+u_2)\cdot]$. Notice that operator receives arguments inside the partial derivative ∂_{xx}. This is represented with a dot inside the square brackets.

Proceeding in the same way with the second term in Eq. (A.5), the adjoint operator becomes

$$\begin{aligned}\mathcal{L}^\dagger = &-\eta + 2\kappa(u_1+u_2) - 3(u_1+u_2)^2 + \delta\partial_{xx} \\ &- \gamma\left\{(u_1+u_2)\partial_{xx} + \partial_{xx}\left[(u_1+u_2)\cdot\right]\right\} \\ &- \alpha\left\{(u_1+u_2)\partial_{xxxx} + \partial_{xxxx}\left[(u_1+u_2)\cdot\right]\right\}.\end{aligned} \tag{A.9}$$

A.2. Kernel of $\mathcal{L}^\dagger$

To apply the Fredholm solvability condition, it is necessary to calculate the kernel components of $\mathcal{L}^\dagger$, that is, the elements that fulfill $\langle f|\mathcal{L}^\dagger = 0$. Due to the complexity of $\mathcal{L}^\dagger$, they are obtained numerically by discretizing its derivatives, using central differencing with the 4 nearest neighbors. Thus, when applying $\mathcal{L}^\dagger$ to a real-valued function f, $\langle f|\mathcal{L}^\dagger$ becomes

$$\begin{aligned}\langle f_j|\mathcal{L}^\dagger = &\left(\frac{7c_4}{240\mathrm{dx}^4} - \frac{7c_3}{240\mathrm{dx}^3} - \frac{c_2}{560\mathrm{dx}^2} + \frac{c_1}{280\mathrm{dx}}\right)f_{j-4} \\ &+ \left(-\frac{2c_4}{5\mathrm{dx}^4} + \frac{3c_3}{10\mathrm{dx}^3} + \frac{8c_2}{315\mathrm{dx}^2} - \frac{4c_1}{105\mathrm{dx}}\right)f_{j-3} \\ &+ \left(\frac{169c_4}{60\mathrm{dx}^4} - \frac{169c_3}{120\mathrm{dx}^3} - \frac{c_2}{5\mathrm{dx}^2} + \frac{c_1}{5\mathrm{dx}}\right)f_{j-2} \\ &+ \left(-\frac{122c_4}{15\mathrm{dx}^4} + \frac{61c_3}{30\mathrm{dx}^3} + \frac{8c_2}{5\mathrm{dx}^2} - \frac{4c_1}{5\mathrm{dx}}\right)f_{j-1} \\ &+ \left(\frac{91c_4}{8\mathrm{dx}^4} - \frac{205c_2}{72\mathrm{dx}^2} + c_0\right)f_j \\ &+ \left(-\frac{122c_4}{15\mathrm{dx}^4} - \frac{61c_3}{30\mathrm{dx}^3} + \frac{8c_2}{5\mathrm{dx}^2} + \frac{4c_1}{5\mathrm{dx}}\right)f_{j+1} \\ &+ \left(\frac{169c_4}{60\mathrm{dx}^4} + \frac{169c_3}{120\mathrm{dx}^3} - \frac{c_2}{5\mathrm{dx}^2} - \frac{c_1}{5\mathrm{dx}}\right)f_{j+2} \\ &+ \left(-\frac{2c_4}{5\mathrm{dx}^4} - \frac{3c_3}{10\mathrm{dx}^3} + \frac{8c_2}{315\mathrm{dx}^2} + \frac{4c_1}{105\mathrm{dx}}\right)f_{j+3} \\ &+ \left(\frac{7c_4}{240\mathrm{dx}^4} + \frac{7c_3}{240\mathrm{dx}^3} - \frac{c_2}{560\mathrm{dx}^2} - \frac{c_1}{280\mathrm{dx}}\right)f_{j+4},\end{aligned} \tag{A.10}$$

with

$$\begin{aligned}c_0 &= -\eta + 2\kappa U - 3U^2 - 2\gamma\,\partial_{xx}U - 2\alpha\,\partial_{xxxx}U, \\ c_1 &= -2\gamma\,\partial_x U - 4\alpha\,\partial_{xxx}U, \\ c_2 &= \delta - \gamma U - 6\alpha\,\partial_{xx}U, \\ c_3 &= -4\alpha\,\partial_x U, \\ c_4 &= -\alpha U\,\partial_{xxxx},\end{aligned} \tag{A.11}$$

where $U = u_1 + u_2$, and $f_j \equiv f(x = \mathrm{d}xj)$, with dx the discretization used.

Finding the kernel of $\mathcal{L}^\dagger$ is equivalent to determining the kernel (or nullspace) of a matrix M that satisfies

$$M\vec{f} = \vec{0} \quad \text{with} \quad \vec{f} = \begin{pmatrix} f_1 \\ \vdots \\ f_{j-1} \\ f_j \\ f_{j+1} \\ \vdots \\ f_N \end{pmatrix}, \tag{A.12}$$

with N the number of points considered in the discretization. Let us first take a look at the eigenvalue spectrum of M. Using $\mathrm{d}x = 0.1$, $N = 30$, and setting u_{LS}^- and u_{LS}^+ at a distance $r = 150$, we obtain the eigenvalue spectrum shown in Fig. A.1(a) and (b). As the graph shows, we confirm the stability of the localized structures as every eigenvalue has a negative real part. Moreover, the lowest eigenvalues (-0.022 and -0.024) decrease as the distance r and the number of points N increase, implying that they correspond to the null eigenvalues we are looking for. They are not exactly equal to zero due to the numerical approximation.

Finally, the linear combination of the eigenvectors associated with the calculated null eigenvalues gives us the elements of the kernel of $\mathcal{L}^\dagger$. These will be labeled as $\langle\tau|$ and $\langle\chi|$. Their respective profiles are shown in Fig. A.1(c) and (d).

A.3. Interaction dynamical equations

Having the kernel of $\mathcal{L}^\dagger$, the dynamical equations of r and x_0 are determined by applying the Fredholm solvability condition. This states that the linear system (A.1) admits solution if and only if

$$\langle\tau|b\rangle = 0 \tag{A.13}$$

and

$$\langle\chi|b\rangle = 0. \tag{A.14}$$

In what follows, we expand both products and obtain dynamical equations for both $x_0(t)$ and $r(t)$.

A.3.1. Equation for the central position $x_0(t)$

In the first of these products, Eq. (A.13), given the form of b (see Eq. (A.3)), and since τ is odd around x_0, the only term that remains is

$$\langle\tau|\dot{x}_0\left(\partial_{z_1}u_1 + \partial_{z_2}u_2\right)\rangle = 0, \tag{A.15}$$

implying that

$$\dot{x}_0 = 0, \tag{A.16}$$

i.e., the central position of the LSs does not move. This result is observed in the numerical simulations, which is expected due to the symmetries of the dynamical equation of the system.

A.3.2. Equation for the distance $r(t)$

On the other hand, in the second product, Eq. (A.14), due to the symmetries of the terms involved, the ones that remain are

$$\begin{aligned} &\langle\chi|(\dot{r}/2)\left(\partial_{z_1}u_1 - \partial_{z_2}u_2\right)\rangle + \\ &\langle\chi|-2\kappa u_1u_2 + 3u_1u_2\,(u_1+u_2) \\ &+ \gamma\,(u_1\partial_{xx}u_2 + u_2\partial_{xx}u_1) \\ &+ \alpha\,(u_1\partial_{xxxx}u_2 + u_2\partial_{xxxx}u_1) = 0. \end{aligned} \tag{A.17}$$

The integrals involved in this equation can be approximated analytically. For this, it is convenient to write

$$\chi(x) = \chi_-(x - x_1) + \chi_+(x - x_2), \tag{A.18}$$

that is, to divide χ into two parts, one localized around x_1 and the other around x_2. To illustrate how to approximate the integrals analytically, let us take a look at the second product of (A.17), i.e.

$$\begin{aligned} \langle\chi|2\kappa u_1u_2\rangle &= 2\kappa\int_{-\infty}^{\infty}\left[\chi^-(x-x_1) + \chi^+(x-x_2)\right] \\ &\quad\times\, u_1(x-x_1)u_2(x-x_2)\mathrm{d}x \\ &= 2\kappa\left[\int_{-\infty}^{\infty}\chi^-(z_1)u_1(z_1)u_2(z_1-r)\mathrm{d}z_1\right. \\ &\quad\left.+\int_{-\infty}^{\infty}\chi^+(z_2)u_1(z_2+r)u_2(z_2)\mathrm{d}z_2\right]. \end{aligned} \tag{A.19}$$

In the second equality, we have changed our variables to $z_1 = x - x_1$ and $z_2 = x - x_2$ in the first and second integrals, respectively. We have also used $r = x_2 - x_1$. These integrals are exponentially close to zero in the whole region of integration, except when they are evaluated near zero. Thus, a good approximation of them is given by setting the integral limits from $-r/2$ to $r/2$. Moreover, since r is large, the terms $u_2(z_1 - r)$ and $u_1(z_2 + r)$ are exponentially small in the region of integration. An approximation of these functions is given then by the asymptotic behavior of u_1 and u_2 (see Eq. (23)), so that

$$\begin{aligned} &\langle\chi|2\kappa u_1u_2\rangle \approx \\ &2\kappa\left[\int_{-r/2}^{r/2}\chi^-(z_1)u_1(z_1)e^{-\beta|z_1-r|}\mathrm{d}z_1 + \int_{-r/2}^{r/2}\chi^+(z_2)e^{-\beta|z_2+r|}u_2(z_2)\mathrm{d}z_2\right]. \end{aligned} \tag{A.20}$$

where $|z_1 - r| = r - z_1$ and $|z_2 + r| = z_2 + r$ in this region of integration. We write

$$\langle\chi|-2\kappa u_1u_2\rangle \approx -2\kappa e^{-\beta r}I_1, \tag{A.21}$$

where

$$I_1 = -\left[\int_{-r/2}^{r/2}\chi^-(z_1)u_1(z_1)e^{\beta z_1}\mathrm{d}z_1 + \int_{-r/2}^{r/2}\chi^+(z_2)e^{-\beta z_2}u_2(z_2)\mathrm{d}z_2\right]. \tag{A.22}$$

Proceeding in the same way with the other integrals in Eq (A.17), we finally obtain the dynamical equation for r

$$\dot{r} = Ae^{-\beta r} + Be^{-2\beta r}, \tag{A.23}$$

where

$$A = \frac{2\left[(\alpha\beta^4 + \gamma\beta^2 - 2\kappa)I_1 + 3I_2 + \gamma I_4 + \alpha I_5\right]}{\langle\chi|\partial_{z_1}u_1 - \partial_{z_2}u_2\rangle} \tag{A.24}$$

and

$$B = \frac{6I_3}{\langle\chi|\partial_{z_1}u_1 - \partial_{z_2}u_2\rangle}, \tag{A.25}$$

with

$$\begin{aligned} I_2 &= -\left[\int_{-r/2}^{r/2}\chi^-(z_1)(u_1(z_1))^2e^{\beta z_1}\mathrm{d}z_1\right. \\ &\quad\left.+\int_{-r/2}^{r/2}\chi^+(z_2)e^{-\beta z_2}(u_2(z_2))^2\mathrm{d}z_2\right], \end{aligned} \tag{A.26}$$

$$\begin{aligned} I_3 &= -\left[\int_{-r/2}^{r/2}\chi^-(z_1)u_1(z_1)e^{2\beta z_1}\mathrm{d}z_1\right. \\ &\quad\left.+\int_{-r/2}^{r/2}\chi^+(z_2)e^{-2\beta z_2}u_2(z_2)\mathrm{d}z_2\right], \end{aligned} \tag{A.27}$$

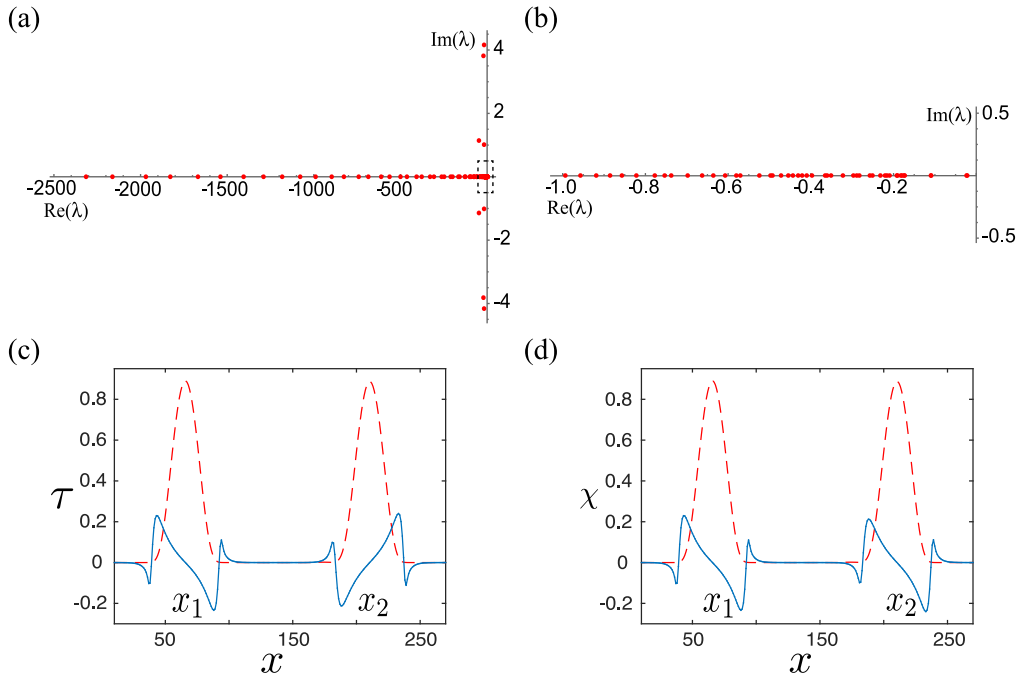

Fig. A.1. (a) Eigenvalue spectrum of matrix M using $\mathrm{d}x = 0.1$ and $N = 30$. (b) Zoom of the dashed region marked in (a). Figures (c) and (d) show the null eigenvector τ and χ (solid line), respectively, and the associated localized structures profile (dashed line). Parameters used are the same as in Fig. 3.

$$I_4 = -\left[\int_{-r/2}^{r/2} \chi^-(z_1)\partial_{z_1 z_1} u_1(z_1) e^{\beta z_1}\mathrm{d}z_1 + \int_{-r/2}^{r/2} \chi^+(z_2) e^{-\beta z_2}\partial_{z_2 z_2} u_2(z_2)\mathrm{d}z_2\right] \tag{A.28}$$

and

$$I_5 = -\left[\int_{-r/2}^{r/2} \chi^-(z_1)\partial^{(4)}_{z_1} u_1(z_1) e^{\beta z_1}\mathrm{d}z_1 + \int_{-r/2}^{r/2} \chi^+(z_2) e^{-\beta z_2}\partial^{(4)}_{z_2} u_2(z_2)\mathrm{d}z_2\right]. \tag{A.29}$$

All these integrals can be calculated numerically. We have checked that factors A and B are positive for the range of parameters used in the simulations.

Appendix B. Derivation of the interaction potential in 2D

In this section, we derive the interaction law for $r(t)$ in two dimensions. The procedure is essentially the same as in one dimension, as we focus on the dynamics of the x axis. The main difference relies on the asymptotic behavior of the localized structures. In fact, the linear system obtained after replacing the ansatz will be

$$\mathcal{L}W = b, \tag{B.1}$$

with the same operator $\mathcal{L}$ as in one dimension, and

$$\begin{aligned} b = &\frac{\dot r}{2}\left(\partial_{z_1}u_1 - \partial_{z_2}u_2\right) \\ &- 2\kappa u_1 u_2 + 3u_1u_2\left(u_1+u_2\right) \\ &+ \gamma\left(u_1\partial_{xx}u_2 + u_2\partial_{xx}u_1\right) \\ &+ \alpha\left(u_1\partial_{xxxx}u_2 + u_2\partial_{xxxx}u_1\right), \end{aligned} \tag{B.2}$$

with $z_\pm = x \mp r/2$. We choose the same inner product as in one dimension, and in consequence, we obtain the same kernel of $\mathcal{L}^\dagger$. These are labeled again as $\langle\tau|$ and $\langle\chi|$.

By applying the Fredholm solvability condition, $\langle\tau|b\rangle = 0$, we obtain that $\dot x_0 = 0$, i.e. there are no dynamics in the center position, as in one dimension. For the second product, $\langle\chi|b\rangle = 0$, the analytical approximations needed are slightly different than in one dimension. To illustrate them, let us consider the inner product between χ and $2\kappa u_1u_2$ (as in Eq. (A.19))

$$\begin{aligned} &\langle\chi|2\kappa u_1u_2\rangle \\ &= 2\kappa\left[\int_{-\infty}^{\infty}\chi^-(z_1)u_1(z_1)u_2(z_1-r)\mathrm{d}z_1 + \int_{-\infty}^{\infty}\chi^+(z_2)u_1(z_2+r)u_2(z_2)\mathrm{d}z_2\right]. \end{aligned} \tag{B.3}$$

Again, we have split χ as in Eq. (A.18). We also restrict the integral limits only from $-r/2$ to $r/2$ and replace $u_2(z_1-r)$ and $u_1(z_2+r)$ by their asymptotic behavior. Since now we are focusing on the dynamics of the x axis, the asymptotic behavior takes the form (see Eq. (29))

$$u_{LS}(|x-x_0|\to\infty) \propto \frac{e^{-\beta|x-x_0|}}{\sqrt{|x-x_0|}}, \tag{B.4}$$

where x_0 is the central position. Thus,

$$\begin{aligned} &\langle\chi|2\kappa u_1u_2\rangle \approx \\ &2\kappa\left[\int_{-r/2}^{r/2}\chi^-(z_1)u_1(z_1)\frac{e^{-\beta|z_1-r|}}{\sqrt{|z_1-r|}}\mathrm{d}z_1 + \int_{-r/2}^{r/2}\chi^+(z_2)\frac{e^{-\beta|z_2+r|}}{\sqrt{|z_2+r|}}u_2(z_2)\mathrm{d}z_2\right]. \end{aligned} \tag{B.5}$$

Notice that $|z_1-r| = r-z_1$ and $|z_2+r| = z_2+r$ in this region of integration. Moreover, performing a Taylor expansion in $z_\pm$, we get

$$\frac{1}{\sqrt{z_\pm \pm r}} \approx \frac{1}{\sqrt r} \pm \frac{z_\pm}{2r^{3/2}}. \tag{B.6}$$

The second term of this expansion can be neglected as r is large. We write then

$$\langle \chi | 2\kappa u_1 u_2 \rangle \approx 2\kappa \frac{e^{-\beta r}}{\sqrt{r}} \left[\int_{-r/2}^{r/2} \chi^-(z_1) u_1(z_1) e^{\beta z_1} dz_1 + \int_{-r/2}^{r/2} \chi^+(z_2) e^{-\beta z_2} u_2(z_2) dz_2 \right], \tag{B.7}$$

i.e., $\langle \chi || 2\kappa u_1 u_2 \rangle \approx 2\kappa \frac{e^{-\beta r}}{\sqrt{r}} I_1$, with I_1 defined as in the previous section. Proceeding in the same way with the other integrals from $\langle \chi | b \rangle = 0$, we get, for large r Eq. (31).

References

[1] E. Meron, Nonlinear Physics of Ecosystems, CRC Press, Taylor & Francis Group, 2015.
[2] V. Deblauwe, et al., Glob. Ecol. Biogeogr. 17 (2008) 715.
[3] O. Lejeune, M. Tlidi, J. Veg. Sci. 10 (1999) 201.
[4] von Hardenberg J., et al., Phys. Rev. Lett. 87 (2001) 198101.
[5] E. Gilad, et al., Phys. Rev. Lett. 93 (2004) 098105.
[6] O. Lejeune, et al., Int. J. Quantum Chem. 98 (2004) 261.
[7] Rietkerk, et al., Am. Nat. 160 (2002) 524.
[8] K. Gowda, Phys. Rev. E 89 (2014) 022701.
[9] G. Getzin, et al., Ecography 38 (2015) 1.
[10] L. Mander, R. Soc. Open Sci. 4 (2017) 160443.
[11] H. Yizhaq, et al., Ecohydrology (2019) e2135, 1.
[12] R. Lefever, O. Lejeune, Bull. Math. Biol. 59 (1997) 263.
[13] O. Lejeune, et al., Phys. Rev. E 66 (2002) 010901(R).
[14] M. Rietkerk, et al., Science 305 (2004) 1926.
[15] E. Meron, et al., Chaos Solitons Fractals 19 (2004) 367.
[16] E. Meron, et al., Chaos 17 (2007) 037109.
[17] P. Couteron, et al., Phil. Trans. R. Soc. A 372 (2014) 20140102.
[18] D. Escaff, et al., Phys. Rev. E 91 (2015) 022924.
[19] M. Tlidi, et al., Lect. Notes Phys. 751 (2008) 381.
[20] C.E. Tarnita, et al., Nature 541 (2017) 398.
[21] D. Ruiz-Reynes, et al., Sci. Adv. 3 (2017) e1603262.
[22] J.D. Murray, Mathematical biology, in: Biomathematics, Vol. 19, Springer, Berlin, Germany, 1989.
[23] M. Tlidi, et al., Chaos 17 (2007) 037101.
[24] E. Knobloch, Chaos 17 (2007) 037102.
[25] E. Knobloch, Nonlinearity 21 (2008) T45.
[26] N. Akhmediev, A. Ankiewicz (Eds.), Dissipative Solitons: From Optics to Biology and Medicine, in: Lecture Notes in Physics, vol. 751, Springer, Heidelberg, Germany, 2008.
[27] L. Ridolfi, et al., Noise-Induced Phenomena in the Environmental Sciences, Cambridge University Press, Cambridge, UK, 2011.
[28] O. Descalzi, et al. (Eds.), Localized States in Physics: Solitons and Patterns, Springer Science & Business Media, 2011.
[29] M. Tlidi, et al., Phil. Trans. R. Soc. A 372 (2014) 20140101.
[30] M. Tlidi, M.G. Clerc, Nonlinear dynamics: materials, theory and experiments, in: Springer Proceedings in Physics, vol. 173, 2016.
[31] Y.K. Chembo, et al., Eur. Phys. J. D 71 (2017) 299.
[32] M. Tlidi, et al., Phil. Trans. R. Soc. A (London) 376 (2018) 20180114, Phil. Trans. R. Soc. A (London) 376 20180276.
[33] A. Mauchamp, et al., Ecol. Model. 71 (1994) 107.
[34] J.M. Thiery, et al., J. Ecol. 83 (1995) 497.
[35] D.L. Dunkerley, Plant Ecol. 129 (1997) 103.
[36] C.A. Klausmeier, Science 284 (1999) 1826.
[37] T. Okayasu, Y. Aizawa, Progr. Theoret. Phys. 106 (2001) 705.
[38] J.A. Sherratt, J. Math. Biol. 51 (2005) 183.
[39] N. Barbier, et al., J. Ecol. 94 (2006) 537.
[40] N. Barbier, et al., Ecology 89 (2008) 1521.
[41] R. Lefever, et al., J. Theoret. Biol. 261 (2009) 194.
[42] A.G. Vladimirov, et al., Phys. Rev. A 84 (2011) 043848.
[43] P. Verhulst, Nouveaux mémoires de l'Académie Royale des Sciences et Belles-Lettres de Bruxelles, 1845, 18 14.
[44] J. Mawhin, Acad. Roy. Belg. Bull. Cl. Sci. 13 (2002) 349.
[45] J. Mawhin, First 60 (2004) 147.
[46] C. Fernandez-Oto, et al., Phys. Rev. Lett. 110 (2013) 174101.
[47] R. Martinez-Garcia, et al., Geophys. Res. Lett. 40 (2013) 6143.
[48] R. Martínez-García, et al., Phil. Trans. R. Soc. A 372 (2014) 20140068.
[49] C. Fernandez-Oto, et al., Phil. Trans. R. Soc. A 372 (2014) 20140009.
[50] P. Colet, et al., Phys. Rev. E 89 (2014) 012914.
[51] L. Gelens, et al., Phys. Rev. E 89 (2014) 012915.
[52] V. Dornelas, et al., Phys. Rev. E 99 (2019) 062225.
[53] D. Escaff, Eur. Phys. J. D 62 (2011) 33.
[54] R. Lefever, J.W. Turner, C. R. Mec. 304 (2012) 818.
[55] J. Cisternas, et al., Chaos Solitons Fractals 133 (2020) 109617.
[56] R.M. Hornreich, H. Luban, Phys. Rev. Lett. 35 (1975) 1678.
[57] M. Cross, P. Hohenberg, Rev. Modern Phys. 65 (1993) 851.
[58] C. Fernandez-Oto, et al., Phys. Rev. Lett. 122 (2019) 048101.
[59] E. Meron, Math. Biosci. 271 (2016) 1.
[60] J. Swift, P.C. Hohenberg, Phys. Rev. A 15 (1977) 319.
[61] R. Richter, I.V. Barashenkov, Phys. Rev. Lett. 94 (2005) 184503.
[62] M.K. Wadee, et al., Physica D (Amesterdam) 163 (2002) 26.
[63] D.W. Hunt, Discrete Contin. Dyn. Syst. Ser. B 3 (2003) 505.
[64] M'F. Hilali, et al., Phys. Lett. A 217 (1996) 263.
[65] B. Golan, et al., Theoret. Ecol. 5 (2012) 591.
[66] I. Bordeu, et al., Sci. Rep. 6 (2016) 33703.
[67] M. Tlidi, et al., Ecol. Indicators 94 (2018) 534.
[68] P. Mandel, et al., Phys. Rev. A 47 (1993) 4277.
[69] M. Tlidi, et al., Phys. Rev. A 48 (1993) 4605.
[70] M. Tlidi, et al., Phys. Rev. Lett. 73 (1994) 640.
[71] Y.R. Zelnik, et al., Phil. Trans. R. Soc. A 371 (2013) 20120358.
[72] Y.R. Zelnik, et al., Ecol. Complex. 25 (2016) 26.
[73] E. Berríos-Caro, et al., Sci. Rep. 10 (2019) 1.
[74] M.G. Clerc, et al., Phys. Rev. E 72 (2005) 056217.
[75] K.A. Gorshkov, L.A. Ostrovsky, Physica D 3 (1981) 428.
[76] I.S. Aranson, et al., Physica D 43 (1990) 435.
[77] A.G. Vladimirov, et al., Phys. Rev. E 65 (2002) 064606.
[78] M. Tlidi, et al., IEEE J. Quant. Elec. 39 (2003) 216.
[79] A.G. Vladimirov, et al., Phys. Rev. A 97 (2018) 013816.